Optical design of the High Resolution Imaging Channel of SIMBIO-SYS

MICHELE ZUSI[1,*], RICCARDO PAOLINETTI[2], VINCENZO DELLA CORTE[3], GABRIELLA MARRA[3,4], MARCO BARONI[2], PASQUALE PALUMBO[4] AND GABRIELE CREMONESE[5]

[1] *Istituto Nazionale di Astrofisica – Istituto di Astrofisica e Planetologia Spaziali, Via del Fosso del Cavaliere 100, 00133 Rome, Italy*
[2]*Leonardo S.p.A., Via delle Officine Galileo 1, 50013 Campi Bisenzio, Firenze, Italy*
[3]*Dipartimento di Scienze e Tecnologie, University of Naples "Parthenope", Centro Direzionale – Isola C4, 80143 Naples, Italy*
[4]*Istituto Nazionale di Astrofisica – Osservatorio Astronomico di Capodimonte, Salita Moiariello 16, 87131 Naples, Italy*
[5]*Istituto Nazionale di Astrofisica – Osservatorio Astronomico di Padova, Vicolo dell'Osservatorio 5, 35122 Padua, Italy*
**Corresponding author: michele.zusi@iaps.inaf.it*

Received XX Month XXXX; revised XX Month, XXXX; accepted XX Month XXXX; posted XX Month XXXX (Doc. ID XXXXX); published XX Month XXXX

This paper describes the optical design of the High Resolution Imaging Channel (HRIC), which is part of the Spectrometers and Imagers for Mercury Planetary Orbiter (MPO) BepiColombo Integrated Observatory SYStem (SIMBIO-SYS) suite, for imaging and spectroscopic investigation of Mercury. The optical design has been optimized to achieve the stringent scientific requirement of 5 m ground sampling at 400 km from the planet surface in the harsh Mercury environment.

OCIS codes: *(110.0110) Imaging systems, (350.6090) Space optics, (110.6770) Telescope, (120.4570) Optical design of instruments, (120.0280) Remote sensing and sensors.*

http://dx.doi.org/10.1364/AO.99.099999

1. INTRODUCTION

SIMBIO-SYS [1] is the primary remote sensing instrument aboard the Mercury Planetary Orbiter (MPO) of the European Space Agency (ESA) mission BepiColombo [2] launched in October 2018 and aimed at the geo-chemical and morphological investigation of the Mercury surface.

HRIC [3, 4] is the High Resolution Imaging Channel of SIMBIO-SYS instrument and together with a STereoscopic imaging Channel (STC) [5] and a Visual and Infrared Hyper-spectral Imager channel (VIHI) [6] will answer fundamental questions related to our knowledge about Mercury.

HRIC has been designed, manufactured and tested by a team involving the Istituto Nazionale di AstroFisica (INAF) (at Istituto di Astrofisica e Planetologia Spaziali (IAPS) in Rome and Osservatorio Astronomico di Capodimonte in Naples), the Parthenope University in Naples and the Leonardo S.p.A. in Florence [7]). This instrument will provide images covering up to 20% of the planet surface with 4 optical filters operating in the visible and near infrared spectral range. In particular, it will observe special surface regions that includes key surface features (e.g., craters, tectonic features, lava flows and plains) whose images will help in the study of their relationship with geological, geophysical and geochemical internal processes, as well as the effect of meteor bombardment.

In this paper we present the adopted configuration for the HRIC optical design and in particular the requirements that guided the optical design is reported in Section 2; Section 3 describes all the main elements of the HRIC optical design; the indexes used to evaluate the image quality of the HRIC optical design are reported in Section 4; Section 5 describes the analyses done for the mounting opto-mechanical tolerances; the straylight analysis in terms of ghosts and scattered light is deeply reported in Section 6 and in Section 7 some conclusions on the HRIC optical design are discussed.

2. HRIC OPTICAL DESIGN AND MANUFACTURING

The HRIC primary task is to provide high resolution images of selected Mercury surface features like craters, scarps, lava flows, plains and hollows both with panchromatic and broad-band filters [8]. The final objective is to produce images at unprecedented detail level in the visible range which can help planetary scientists (i.e., geologists and planetary formation modelers) in the correct interpretation of the present Mercury surface morphology and mineralogical composition and in the reconstruction of its origin and evolution throughout the early stage of the Solar System history.

From these scientific objectives derive a list of stringent optical requirements that has been summarized in Table 1.

Table 1. Performance requirements affecting HRIC optical design.

Parameter	Description
On-ground resolution	< 10 m/pxl from 400 km of altitude
Field of View	> 1 deg (squared)
Spectral range	400-900 nm
Pupil diameter	> 80 mm
Filters	1 panchromatic + 3 colour filters
Optical MTF at Nyquist frequency	≥ 0.3 (at λ=632.8 nm)

The above listed parameters are derived from the analysis of the scientific requirements (e.g., pixel scale, spectral range) coupled with the expected flux (i.e., solar constant, Mercury albedo).

Following the above listed general requirements, a preliminary optical design was studied [8, 9] that has been deeply analyzed and optimized with the collaboration of Leonardo S.p.A. in the optical project presented in the following paragraphs. The resulting design is capable of satisfying high-performance requirements, related primarily to image resolution and quality over the covered Field of View (FoV), with a very compact envelope (297x214x212 mm^3, excluding external baffle) and mass (2.7 kg, excluding external baffle).

A. Telescope

1. Layout

The HRIC layout (Figure 1) is based on a catadioptric optical design and consists of an optimized Ritchey–Chrétien configuration with a dedicated corrector.

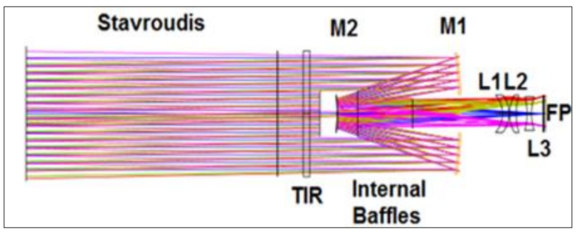

Figure 1: HRIC optical layout with TIRD filter (TIR), the two mirrors (M1 and M2), three-lens (L1, L2 and L3) corrector plus filters deposited on the detector window (FP).

Table 2 reports the optical prescriptions of the HRIC layout.

Table 2: HRIC optical design prescription.

Surf nbr	Surface [mm]	RoC [mm]	TH [mm]	Conic Cnst
0	OBJ	Inf	Inf	
1	M1 - stop	-298.5	-111	-1.094
2	M2	-96.56	150.6	-3.097
3	L1 s1	-20.933	6	
4	L1 s2	-22.59	0.5	
5	L2 s1	28.038	6	
6	L2 s2	47.142	10	
7	L3 s1	-41.025	4	
8	L3 s2	37.32	12.5	
9	Image	Inf		

The two mirrors have hyperboloid profiles and have been designed together with the corrector lenses to correct the residual aberration of the Ritchey–Chrétien configuration, i.e., the astigmatism and the FoV curvature aberrations on the 2048 x 2048 pixels detector with a pixel size of 10 µm.

The instrument has a focal length of 800 mm that guarantees the satisfaction of the high spatial resolution requirements. The pupil aperture located on the primary mirror is about 90 mm respecting dimensioning constraints coming from the satellite accommodation while allowing good imaging performances both in terms of Modulation Transfer Function (MTF) and radiometry. The resulting configuration is diffraction limited at 400 nm and with an F-number of F#8.9.

To reduce the light loss due to the central obscuration, the diameter of the secondary mirror has been minimized to about the 30% (in diameter) with respect to the primary mirror resulting in a good energy transfer to the telescope exit pupil.

Distances between optical elements and detector window have been optimized considering the maximum allowable distance (from mounting tolerance analysis – [10]) of the last corrector element from the detector window, and the maximum acceptable image quality degradation on the focal plane.

The optimization of the HRIC telescope has been driven by the possibility to achieve the required alignment of the optical elements by means of opto-mechanical tolerances only. A dedicated fine alignment is required only for the secondary mirror to reach the defined focus position and for the detector which can be translated and tilted to achieve the best fitting of the focal plane position within the entire field of view.

Finally, to compensate the thermomechanical distortions coming from the 100 / 700 K (night / day) thermal gradients expected around Mercury [11], a deep study on proper materials for manufacturing has been done; as a result, for all dioptric and catoptric elements Fused Silica has been used; for the telescope mechanical structure INVAR has been selected; for lenses support, spacers and Focal Plane Assembly (FPA) mechanics Titanium has been adopted.

2. Mirrors and lenses corrector

The HRIC primary mirror has been manufactured by Zeiss, while the secondary mirror and corrector lenses were manufactured by Leonardo S.p.A. (Figure 2).

Figure 2: HRIC manufactured optics mounted with internal baffles, mechanical structure (dark grey arms) and corrector holder (light grey cylinder on the left).

The mirrors have been coated with an enhanced high reflectivity Ag protected coating designed by Leonardo for which reflectance curves are shown in Figure 3 at 0° and 30° Angle Of Incidence (AOI) respectively.

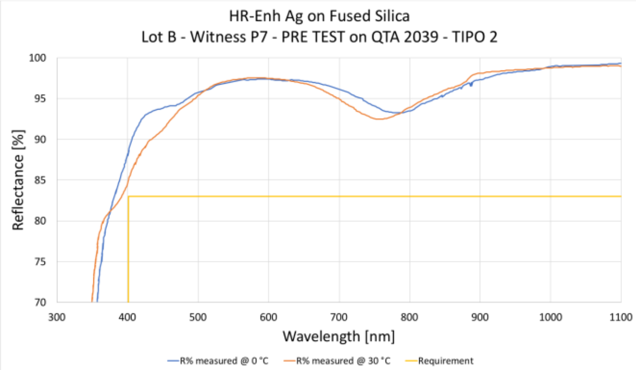

Figure 3: HRIC mirrors reflectance comparison between requirement (yellow line) and measured one at 0° and 30° angle of incidence (blue and red respectively).

The lenses have been coated with an Anti-Reflecting (AR) coating designed by Leonardo for which reflectance curves at 0° and 30° AOI are shown in Figure 4.

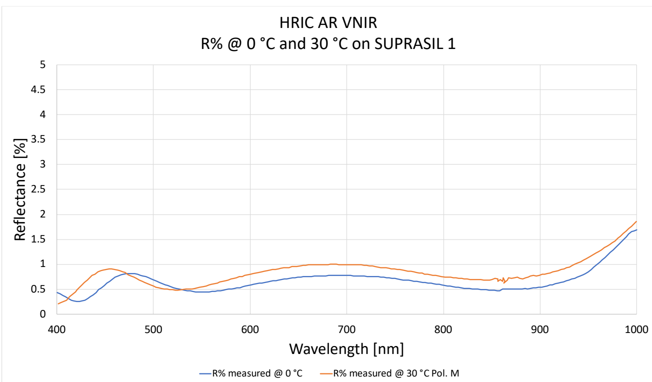

Figure 4: Corrector lenses manufactured coating curves at 0° and 30° AOI.

The thickness of the lenses has been minimized as much as possible to limit absorption losses while assuring structural integrity and respecting the optical shape requirements in terms of optical power and astigmatism. To simplify the manufacturing, all the surface shapes of the corrector lenses have been made spherical and have been optimized using test radii of the manufacturer. The selected glass material is Suprasil 1 which optimizes the system transmittance in the used spectral range and guarantees the needed radiation hardness.

3. TIRD

To reduce the thermal gradients on the optical elements a Thermal Infrared Rejection Design (TIRD) filter with a transmitted wave front error RMS ≤ 230 nm has been placed in front of the instrument Figure 5.

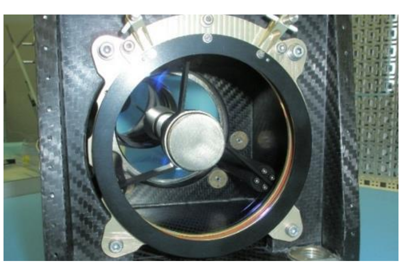

Figure 5: HRIC Camera front view, with TIRD filter (dark grey disk) before secondary mirror support.

This filter is made of a BK7-G18 substrate with anti-reflection coating to reject the infrared radiation coming from space (i.e., Mercury for HRIC). Figure 6 reports a comparison in transmittance and reflectance performance of Indium Tin Oxide (ITO) and Zinc Aluminum-doped Oxide (ZAO) coating designs that have been considered in the optimization process with final adoption of ITO one.

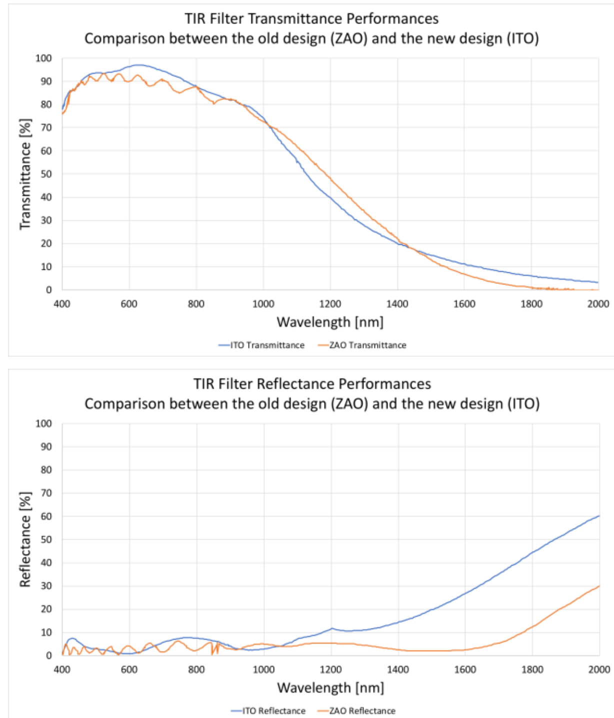

Figure 6: Comparison between ZAO and ITO transmission (above) and reflection (below) profile considered for the TIRD.

4. Filters

For detailed observation of the Mercury surface a panchromatic filter has been selected operating in the whole spectral range (i.e., 400 – 900 nm) while for observations in scientifically relevant wavelength ranges, three band-pass filters (550, 750 and 880 nm as central wavelength and 40 nm of bandwidth) are used. The filters are deposited directly on the detector window, in four strips separated by stripes of absorbing mask which prevents ghosts and separate the different filter areas on the detector well (Figure 7). Filter strip coordinates have been computed by ray tracing, including margin for alignment tolerances and for the enlargement of the beam from the filter to its projection on the detector due to the non-telecentric design.

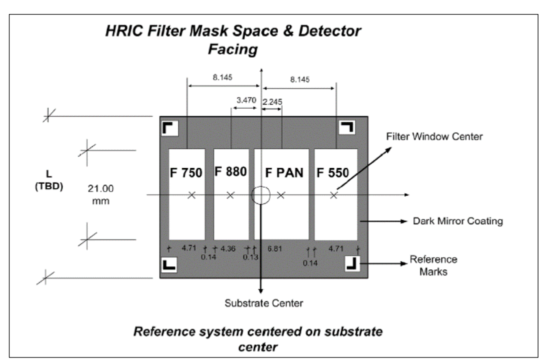

Figure 7: Filter strips dimension specification for manufacturing (view from top).

Because the HRIC optical design is diffraction limited at 400 nm, the F880 filter has been placed as close as possible to the center of the focal plane in order to limit its further reduction which can occur at the edge of the FoV.

Table 3 summarizes the measured transmission efficiencies measured for all filters evidencing the very good performances when compared with the specifications.

Table 3: Summary of the filter specifications and performances.

Specification vs. Measured (red) values				
	FPAN	**F550**	**F750**	**F880**
λ_C [nm]	650 ± 11 652.3	550 ± 6 549.3	750 ± 9 752.9	880 ± 11 880.1
$\nu_{on/off}$ [nm]	400/900 399.8/904	530/570 529.8/570.2	730/770 733.7/773.3	860/900 861.7/901.5
$\Delta\lambda$ [nm]	500 ± 5 504.9	40 ± 2 40.4	40 ± 2 39.6	40 ± 2 39.8
T_p [%]	> 85 98.6	> 80 99.1	> 80 99.7	> 80 98.9
T_o [%]	< 0.05 0.018	< 0.05 0.013	< 0.05 0.012	< 0.05 0.009
T_o/T_i [%]	< 0.005 0.0001	< 0.01 0.002	<0.01 0.002	< 0.01 0.0011
Slope [%]	< 2 1.3	< 2 0.6	< 2 0.6	< 2 0.1

λ_C: Central wavelength
$\Delta\lambda$: Full Width Half Maximum (FWHM)
$\nu_{on/off}$: 50% transmittance cut-on / cut-off wavelength
T_o: mean of out of band transmittance
T_i: mean of in band transmittance
T_p: peak of in band transmittance
Slope: ratio between up / down warding profile and filter band

5. Overall optical transmission

The optical transmittance of the telescope has been calculated considering the reflectivity of the enhanced silver protected coatings provided by Leonardo and applied on the primary mirror and secondary mirror, and the transmittance of the AR coating applied to the corrector lenses and detector window. Furthermore, the transmittance of the TIRD, the interferential filters and the transmittance of the Fused Silica is considered. Finally, the Obstruction Loss is calculated.

In Figure 8 the optical transmission of the telescope mirrors, lenses, TIRD and obstruction are shown with a good (> 40%) global optical transmission (orange line) over the whole spectral range.

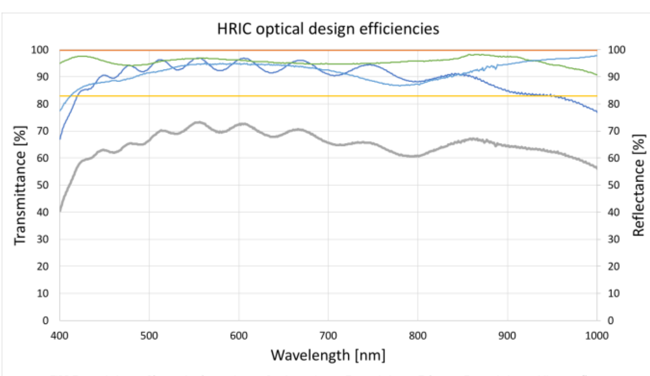

Figure 8: HRIC Optics reflectance/transmission efficiencies.

In Figure 9 the global transmission curve is highlighted and annotated with the global spectral efficiencies of the narrow band and panchromatic filters.

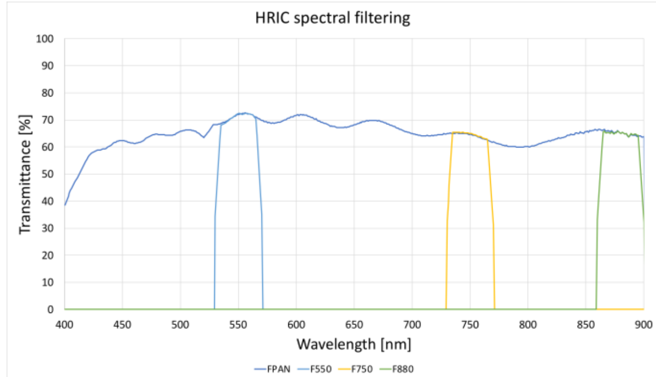

Figure 9: HRIC global optical transmission for all the spectral filters in panchromatic range (i.e., 400-900 nm).

B. Baffles

An external baffling system protects the camera optical entrance reflecting the out-of-field radiance coming from Mercury surface (Figure 10).

The adopted solution is based on a Stavroudis geometrical concept and a heat-rejection front ring which guarantees good optical performances in terms of out-of-field rejection and optimal protection against the heavy thermal load coming from the planet surface [12-14].

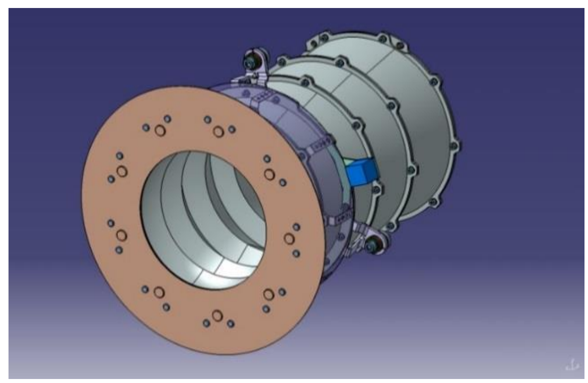

Figure 10: HRIC external baffle cad design.

To attenuate the straylight effect on image, an internal baffle system has been designed minimizing its impact on signal loss and image quality reduction. This system consists of absorbing conical vanes placed around M2 and M1 hole that prevents near out-of-field straylight and diffused (within the HRIC housing structure) to reach the detector (Figure 11). The global optical obscuration moves from 30% due to the secondary mirror to about 41% which represents a limit value to have good image quality in terms of MTF and Signal-to-Noise Ratio (SNR). Being decoupled by the camera, the external baffle diameter has been oversized to tolerate possible distortion of the satellite mounting bracket and alignment tolerances. As a consequence also the internal baffles longitudinal dimensions have been slightly increased with respect to the original design, with no impact on section area (i.e., without increasing obscuration and/or decreasing MTF) and only a small vignetting of the marginal field of view (Figure 11).

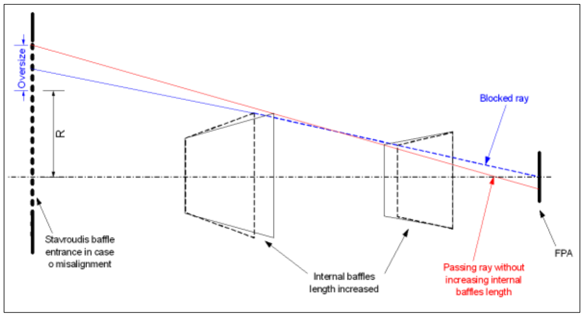

Figure 11: HRIC Internal baffles design modification to prevent stray light.

C. Detector

The selected 2048 x 2048 detector is a hybrid Si-PIN CMOS device with 10 µm pixel pitch, developed by Raytheon Vision System with very high performances in terms of low power consumption and high readout speed, dynamic range and radiation hardness which ensure required performances to the system.

D. Overall performance specification of the HRIC design

To meet the scientific objectives of high spatial resolution imaging an advanced optical design has been developed; this design is capable to work with high thermal gradients foreseen around Mercury without degrading image quality.

Above described optical elements together with the selected and adopted design solutions resulted in an optical configuration for HRIC with the main characteristic reported in Table 4.

Table 4: HRIC main characteristics.

Parameter	Description
Optical configuration	Ritchey–Chrétien modified with corrector
Corrector	Refractive spherical surfaces
Spectral Range	400 – 900 nm
Entrance pupil diameter	89 mm
Angular field of view	1.47° x 1.47°
F-number	8.9
Focal length	800 mm
IFoV	12.5 µrad/pxl
Corrector lenses material	Suprasil 1
CMOS matrix	2048 x 2048
CMOS pixel size	10 µm x 10 µm
CMOS fill factor	100%
CMOS dynamic	120 ke-

The adopted HRIC design when compared to the requirements listed in Table 4, fully satisfies the objectives especially in terms of image resolution providing images with 5 m/pxl of on-ground pixel scale from 400 km of altitude.

3. IMAGE QUALITY

A. Optical performance

Because the system diffraction limited, the fraction of diffraction Ensquared Energy (EE) enclosed in one pixel has been considered to evaluate the image quality. Another parameter that has been considered is the image contrast that has been evaluated by means of the diffraction MTF. For both diffraction EE and MTF evaluation, central obscuration, spiders and baffles obscuration have been included in the analyses. In addition, RMS spot radius on the image plane, field curvature and distortion, have been evaluated.

Main optical performances are reported in Table 5, with a comparison between nominal MTF for manufacturing (with internal baffle and M2 spider) and measured (in red) parameter values after alignment, bonding and vibration tests.

To note that:

- all the measures have been done using an interferometer at 632.8 nm and without considering filters efficiency and detector contributes;
- "as per design" values have been obtained by means of the software OpticStudio by Zemax LLC [15].

*Table 5: HRIC main optical performances comparison between design or manufacturing and measured **(red)** values.*

	Optical performances		
Diffraction EE in one pixel	53% 51%		on axis edge of the field
MTF at Nyquist frequency	40% 37%	39% 33%	on axis edge of the field
RMS spot diameter	2 µm 2.6 µm		on axis edge of the field
Field curvature	0.042 mm		edge of the field
Distortion	0.06 %		edge of the field

The Fraction of the EE curve together with the Diffraction MTF profile of the system are shown in Figure 12 for different FoVs from the centre to the edge (to note that due to the symmetry in the design, [0 1.037] and [0 -1.037] degree profiles of Figure 12 overlap each other).

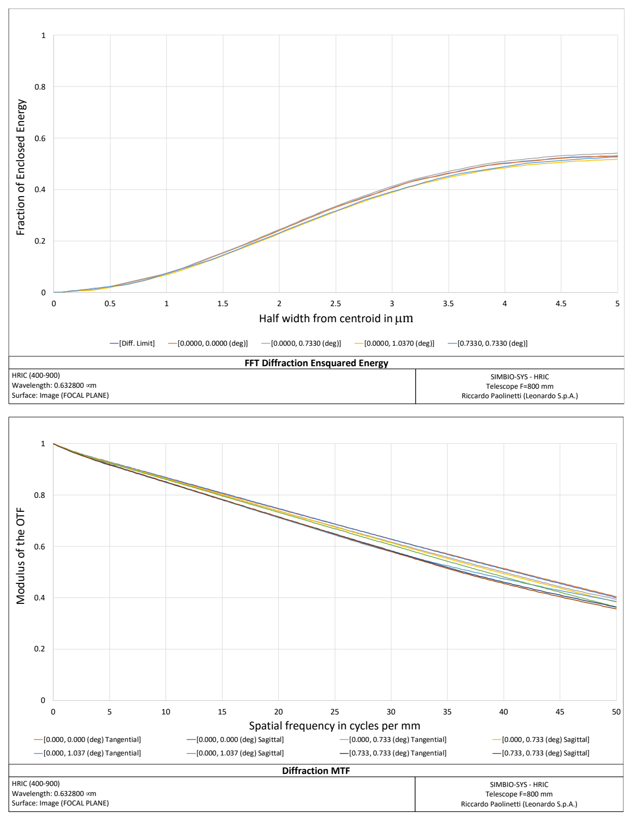

Figure 12: Fraction of EE (above) and Diffraction MTF curves at 632.8 nm (below) for the optical design.

Figure 13 reports the comparison between the "as per design" and the measured diffraction MTF curves for different FoVs from the centre to the edge and after the alignment, bonding and vibration tests.

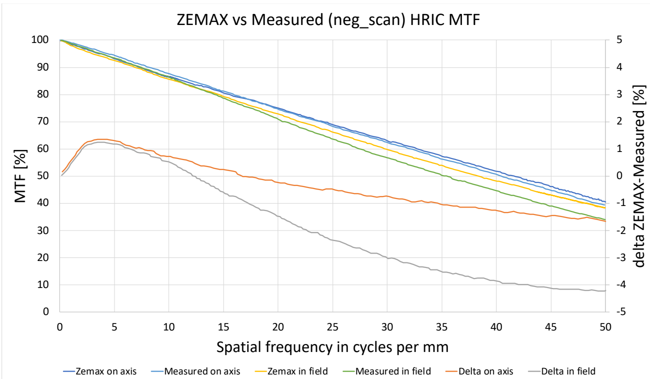

Figure 13: Diffraction MTF curves (by design vs. measured one).

To note, the obtained optical MTF is quite aligned to "as per design" value (Table 5 and Figure 13); nevertheless to verify the real instrument resolution performances, the detector MTF of 50% must be considered determining the final overall optical performance. As a result, the system MTF of the HRIC channel goes down to about 16-18% that is, once compared to other similar high resolution imaging systems [16], a very good result that, together with the application of image post processing techniques (i.e., contrast enhance, PSF removal, smearing compensation), guarantees the satisfaction of the HRIC scientific objectives.

The spot diagrams on the image plane, for different angular distances from the centre to the edge of the field are shown in Figure 14. To note that due to the rotational symmetry of the system, the spot diagram for [0.733, 0.733] degree is just a rotated version of [0, 1.037] degree. Finally, it can be seen that it remains well within 1 pixel moving from 2.6 µm in the centre to about 7.8 µm at the edges of the FoV.

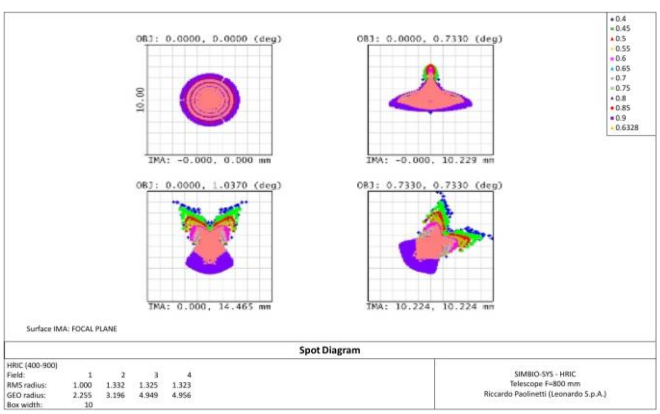

Figure 14: Spot diagrams on the image plane.

The curves of field curvature and percent distortion with respect to the FoV are shown in Figure 15.

The field curvature is less than 0.044 mm and the maximum distortion is 0.06%. Considering that the HRIC FoV depth is about 0.077 mm (=2.44λF#) and that all the field curvatures are within this value, the focal plane can be considered flat.

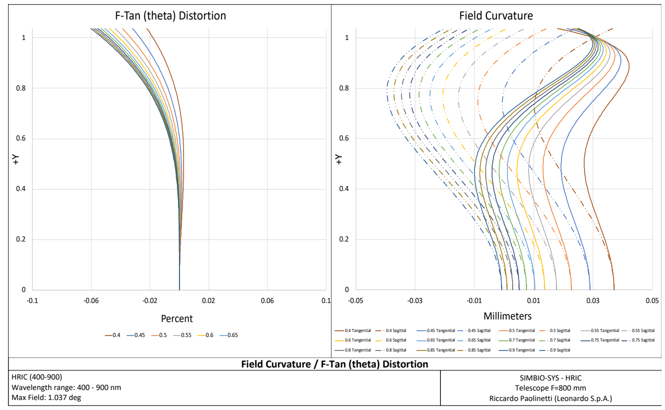

Figure 15: Field curvature in mm (left) and percent distortion (right) between 0.4 (blue) and 0.95 (violet) µm (with 0.05 µm as spectral step) from the line of sight (Y=0°) to the edge of the FoV (Y=1.037°) with step of 0.1°.

B. Ghost analysis

The Optical ghost analysis for HRIC has been performed from 400nm to 900nm spectral range, in the whole FoV computing the raytracing only for the first two bounce between refractive and reflective optical surfaces. This assumption allowed to verify the effective intensity of the ghosts generated just by the dioptric surfaces. In Figure 16 the optical surfaces which contribute to ghosts are shown.

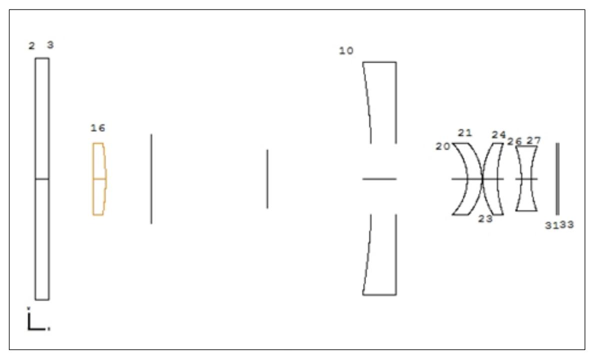

Figure 16: HRIC surfaces layout for ghost analysis.

The relative intensity of the ghost signal on the focal plane has been computed by means of the following:

$$I = \frac{D_{img}^2}{D_{ghost}^2} \cdot R^2 \cdot \left(1 - V_r^2\right) \qquad (1)$$

where D_{img} represents the nominal spot diameter (1 µm), D_{ghost} is the primary ghost spot diameter, R is the average reflectivity of AR coating (0.8%) and V_r is the minimum ghost vignetting ratio computed from axis to maximum FoV.

Table 6 lists the optical elements that generates the ghosts with the highest (i.e., > 10^{-10}) intensity ratio on the focal plane.

To note that surface 32 and 34 are dummy surfaces and they are not considered in the ghosts analysis. In addition, surface 34 represents the detector whose reflectivity has been fixed to 100%.

Table 6: HRIC ghost with highest intensity ratio on the focal plane.

Surface couple	D_{ghost} [mm]	V_r	I
3 vs 2	0.001506*	0.50242	**7.03E-06**
27 vs 24	0.013	0.00001	**3.81E-07**
32 vs 31	0.042043	0.00001	**3.64E-08**
34 vs 31	0.12277	0.00001	**4.27E-09**
34 vs 32	0.081507	0.00001	**9.69E-09**

* The ghost image goes far from the telescope focal plane (about 0.0371 mm).

4. OPTICAL TOLERANCE ANALYSIS

The driving concept for the HRIC telescope design was the mechanical / optical tolerance analysis since every optical element, apart from the secondary mirror and the detector, must be positioned without adjustments.

In case of a Ritchey-Chrétien telescope, in absence of operative focusing, the most sensitive part is the distance stability between primary and secondary mirror which is, in case of HRIC, particularly critic due to the 5x magnification between the telescope and the primary mirror focal length and the defocus of 29x (i.e. a displacement of 1µm between M1 and M2 produces a defocus of 0.029 mm which is of the same order of magnitude of the focus depth).

A preliminary tolerance analysis done at design level [10] has been revised and updated considering all tolerances of manufacturing, mounting and alignment, a Monte Carlo analysis with 1000 run has been done. To each optical element several perturbations (i.e., Curvature Radius, Conic Constant, Thickness or distance, Power fringes, Irregularity fringes, Surface Decenter, Element Decenter, Surface tilt, Element tilt, Index of Refraction, Glass Dispersion) have been applied. The ranges for the perturbation used in the analyses have been obtained considering the real tolerances achievable by the manufacturing processes. The manufacturing and mounting tolerances are shown in Table 7 and Table 8 respectively.

Table 7: Manufacturing tolerances.

ID	Radius [mm]	Thick [mm]	Irregularity [fringes]	Dec [mm]	Tilt ["]
M1*	±0.1	±0.1	0.2	0.015	20
M2	±0.04	±0.1	0.2	0.015	20
L1	±0.02	±0.05	0.5	±0.033	±60
L2	±0.02	±0.03	0.5	±0.033	±60
L3	±0.035	±0.1	0.5	±0.033	±60
Filter	**none**	±0.05	±1	±0.010	±60
TIRD	none	±0.05	0.2	±0.1	±60

* Circularity of ±0.005 mm.

Table 8: Mounting tolerances.

ID	Dec [mm]	Tilt ["]
M1	± 0.005	±20
M2	± 0.005	±20
L1	±0.025	±60
L2	±0.025	±60
L3	±0.025	±60
Filter*	±0.01	±60

Dist [mm]	Tol [mm]
M1-M2	±0.001
M1-L1	±0.05
L1-L2	±0.05
L2-L3	±0.05
Filter-FPA	±0.01

* Parallelism between filter strips longer edges: ±60"

Notice that the mirror mounting tolerances are very tight to guarantee the required image quality.

In Table 9 the sensitivity tolerance analysis summary for the complete optical system is reported in terms of RMS spot radius. This study was performed looking at RMS spot radius change with respect to the nominal design values, for the different line of sight from the center to the edge and considering the M2 position as compensator: M2 can be adjusted along the optical axis of ±0.5 mm with sensitivity of 0.001 mm. In the two orthogonal directions the adjusting range is 0.3 mm with sensitivity of 0.001 mm. The tilt range is ±10 arcmin with sensitivity of 1 arcsec.

The detector position is adjustable along 3 axes to maximize the performance in all points of the FoV; in particular, it can be moved along the optical axis of ±2 mm with a sensitivity of 0.01mm and in the two orthogonal directions of ±0.25 mm with a sensitivity of 0.003 mm.

Table 9: Summary of sensitivity analysis.

Field	RMS spot radius	Change of RMS spot radius
0°	0.0008	0.0004
1.037°	0.00145	0.0013
-1.037°	0.00145	0.0013

Notes:
- all data are in mm.
- changes in back focus is ± 0.2 for all field positions.

The inverse sensitivity is reported in terms of MTF degradation at the Nyquist frequency of 50 cycles/mm for the different FoV in Table 10.

Table 10: Performance of HRIC polychromatic MTF at Nyquist spatial frequency of 50 cycles/mm.

Field	Nominal ave MTF	MTF design + toll
0°	0.399	0.39874126
1.037°	0.36	0.33845660
-1.037°	0.3605	0.31003578

Note: compensator range is ± 0.2 for all field positions.

Obtained results of Table 9 and Table 10 are in a good agreement between the values of design and those measured after manufacturing, alignment and test of the integrated camera respecting the maximum allowed degradation of 4% for both quality indexes.

5. THERMAL ANALYSIS

The stability of the relative position of M1 with respect to M2, mainly in terms of distance between them, and the effect of radial gradients on the optical properties of TIRD filter have been evaluated considering the effect in terms of MTF; the analysis has considered the optical parameter variation (e.g., the refractive index, as function of the temperature) and the following constrains on materials:

- Mirrors (i.e., M1 and M2) made of Fused Silica HOQ 310.
- Lenses L1, L2, L3 made of Fused Silica Suprasil 1.
- TIRD Filter Made of BK7 G18.
- Telescope Mechanical structure made of Invar.
- Lenses and Detector support made of Titanium.

In addition, the following assumptions have been considered:

- constant temperature (i.e., 20 °C applied to all elements);
- operative gradients temperature (coming from instrument thermal analysis);
- radial gradients on the TIRD Filter.

To analyze the performances at -20°C ≤ T ≤ +50°C temperature range, the MTF parameter has been used. It has been computed on the common focal plane for all FoV and for all spectral range, without any focusing adjustment with respect to the nominal condition.

Figure 17 reports the telescope polychromatic MTF evolution at -20°C and at +50°C in both tangential and sagittal direction from the centre to the edge of the HRIC FoV. The black curve is relative to the diffraction limited while the colored curves are relative to some points of FoV from the line of sight to the maximum FoV.

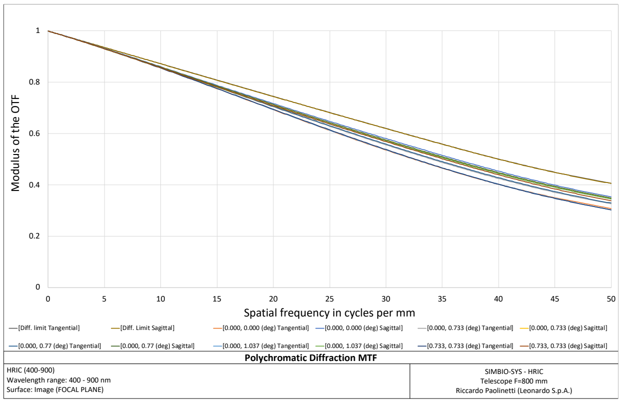

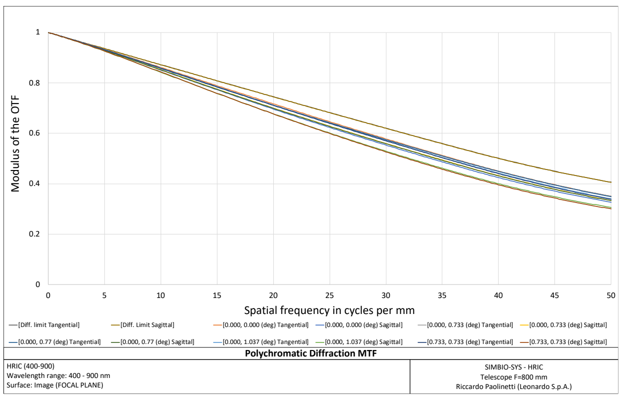

Figure 17: Polychromatic tangential and sagittal MTF at -20°C (above) and +50°C (below) in the centre and at the edge of FoV. The black curve is relative to the diffraction limited while the colored curves are relative to some points of FoV from the line of sight to the maximum FoV.

Figure 17 demonstrates that the MTF degradation for thermo-elastic effects is less than 2.1% with respect to the nominal value.

6. STRAYLIGHT ANALYSIS

A. General assumptions

Straylight is one of the most complex noise contributors to images that depends both on the optical design of the instrument and on the observed scene radiance. It consists of all kinds of undesired light that strikes the detector both from in-field or out-of-field sources. It can be produced either by:

- Refractive surfaces reflection (Ghost). Each ghost image can be characterized by its irradiance (or its total power) and its size.
- Scattered light. Light impacting on the FPA and due to scattering either by micro-roughness of the optical surfaces or by contamination or by any other (illuminated) mechanical object.

To guarantee the satisfaction of the absolute and the relative radiometric accuracy requirements, HRIC straylight effects must be minimized; to this aim, the TIRD + overall system straylight attenuation, defined as the ratio between the total Out-of-Field (OoF) irradiance at TIRD entrance to the irradiance at FPA, shall be such that the following requirements are satisfied:

- Stray light contribution to signal shall remain below 3% (averaged) or average stray light + σ_{str} shall remain below 5% of signal.
- SNR reduction due to stray light is limited to 10% with respect to the value with no stray light contribution. The reference SNR shall be computed considering the photon noise and PRNU at 1%, while stray light effect shall be considered through its photon noise and stray light fluctuation on the frame. For the SNR evaluation, the reference signal is due to 1/20 of the mean irradiance.

To verify the satisfaction of above requirements several simulations have been performed considering an extended source (12' divergence to minimize the diffraction effects) and a 3%/20 as the ratio between straylight and signal irradiance.

B. Scattering analysis

1. Assumptions

The scattered radiation on HRIC detectors may originate from the following elements:

- Optics (roughness, contamination, local defects and filter leakage), whose scattered radiation directly reaches the instruments detector;
- Mechanical parts around M1, M2, L1, L2 and L3;
- Mechanical parts around the detector;
- Mechanical part of the chassis. In this case straylight radiation reaches the detector after at least 2 bounces on mechanical parts.

Regarding the roughness and PArticulate Contamination (PAC) we assumed the following properties for the optics and the mechanics:

- roughness: the models used for roughness are the modified Harvey-Shack BRDF/BSDF whose parameters are reported in Table 11.

Table 11: Harvey models for optical surface roughness.

b	s	l	λ (nm)	(values in RMS)
1.36436154	-2.0	0.01	400	Mirrors 20 Å
0.15018643	-2.0	0.01	400	TIRD 25 Å
0.01884602	-2.0	0.01	400	Lenses 10 Å (f_silica)
0.26950351	-2.0	0.01	900	Mirrors 20 Å
0.02727437	-2.0	0.01	900	TIRD 25 Å
0.00343754	-2.0	0.01	900	Lenses 10 Å (f_silica)
34.1090385	-2.0	0.01	400	STAVROUDIS 100 Å
6.73758786	-2.0	0.01	900	STAVROUDIS 100 Å

- PAC: to compute the contribution of the contamination we assume that:
  - particles scatter according to Mie theory (particles should be separated at least three times their radius);
  - backscattered radiation is not considered;
  - the particle-contaminant size distribution follows the one defined by MIL-Spec 1246b for a Cleanliness Level (CL) (also IEST-STD-CC1246D) where:

$$PAC = \frac{10^{(-7,245+0,962 \cdot log_{10}^{2}(CL))}}{100} \qquad (2)$$

The Harvey-Shack models fitting the BRDF of the Mie contamination for CL300 are reported in Table 12 whose the A, B, C and D contributes are summed in ASAP software [17] for the best fit of the MIE BRDF.

Table 12: Harvey model to fit Mie particles scattering.

b	s	l	λ (nm)	
0.4481	-2.8225	0.0079	400	CL300 1 A
0.0001	-0.5877	0.0268	400	CL300 2 B
0.2576	-2.2974	0.0084	900	CL300 1 C
0.0002	-2.0236	0.3648	900	CL300 2 D

Note: for the mechanics straylight suppression the elettrodag502 treatment has been selected.

Finally, for the analysis of the straylight effects on HRIC we defined the following groups of sources depending on their proximity with respect to the FoV:

1. Infield, that are sources located in the actual FoV of the telescope and whose radiation directly reaches the detectors;
2. Near infield, that are sources that illuminate the telescope optical elements, but their radiation is stopped by baffles before reaching the detector;
3. Out of field, that are source whose is completely stopped by the baffle in front of the telescope but can reach the detector only after a second diffusive bounce on mechanical elements or after two bounces on optical components. In the case of HRIC the contribution of these sources is negligible with respect to the other ones.

2. Infield analysis

The main contributions to infield straylight (half cone angle ≤ 1.037°) are listed in the following table as the ratio between the Straylight and the scientific signal magnitude.

Table 13: Major contributions to infield stray light.

Stray/signal	400 nm	900 nm
Mirror M1	$4.34\cdot10^{-5}$	$1.11\cdot10^{-5}$
Mirror M2	$1.03\cdot10^{-4}$	$2.15\cdot10^{-5}$
Lens L1	$1.03\cdot10^{-5}$	$1.75\cdot10^{-6}$
Lens L2	$1.22\cdot10^{-5}$	$2.26\cdot10^{-6}$
Lens L3	$1.087\cdot10^{-5}$	$2.11\cdot10^{-6}$
Filter TIRD	$4.40\cdot10^{-5}$	$8.65\cdot10^{-6}$
Baffle M1	$6.78\cdot10^{-5}$	$6.64\cdot10^{-5}$
Baffle M2	$2.34\cdot10^{-6}$	$2.29\cdot10^{-6}$
Support of lenses	$2.19\cdot10^{-5}$	$1.99\cdot10^{-5}$
Ferrule of lenses	$2.92\cdot10^{-5}$	$2.65\cdot10^{-5}$

All the other parts not in Table 13 give contribute lower than 10^{-6} / 10^{-7} with respect to the signal.

The total scattering is $5.8\cdot10^{-4}$ at 400 nm and $3.9\cdot10^{-4}$ at 900 nm with respect to the signal (ratio between stray-light and signal irradiance).

The source has an angular extent of 0.1°. The irradiance map due to scattering is reported in Figure 18, where the color scale has been adjusted to enhance straylight (central spot is saturated).

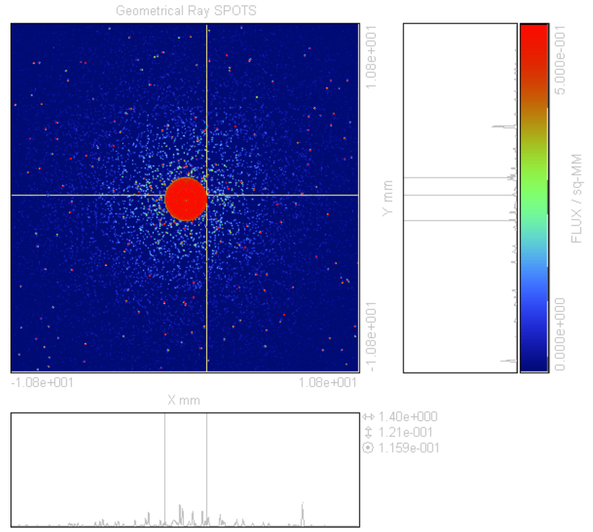

Figure 18: Extended source image with scattered light enhanced.

3. Near-infield analysis

This analysis has been done for source flux AOI between 1.037° and 15.0° at 400 nm. These values represent the field angle value and cut-off angle value. In this situation the light cannot reach directly the detector but illuminates part of the first optics. Scattered light from illuminated optics can reach the detector.

Contribution to near infield stray light from optical elements is negligible and is reported in Table 14.

Table 14: Fraction of flux coming from different object.

Object	Scatter fraction
Stavroudis	$5.41\cdot10^{-6}$
TIRD	$2.14\cdot10^{-5}$
M1	$1.68\cdot10^{-5}$
M2	$1.67\cdot10^{-7}$
Lenses	$4.42\cdot10^{-7}$

Total near infield stray light inclusive of the mechanical parts is $2.8\cdot10^{-4}$ and it is of the same order of the infield source.

4. Out-of-field analysis

This analysis has been done for source with AOI over the 15.0° at 400 nm. This value is the cut-off angle value due to external baffle. In this situation the light cannot reach directly the optics. Only the light scattered from the external baffle can reach the focal plane.

The radiation scattered from baffle a first time and re-scattered a second time by the first optics and mechanics has been also considered with respect to the signal of infield source as reported in Table 15.

Table 15: Ratio of the flux out of cut off reaching detector.

Intermediate count	Ratio
Scattered 1 times	$3.2\cdot10^{-5}$
Scattered 2 times	$1.6\cdot10^{-8}$
TOT	$\mathbf{3.2\cdot10^{-5}}$

5. Contamination analysis

Scattered straylight simulations have been done considering the scattering due to the contamination on the HRIC optical surface expected from the Cleanliness and Contamination Control Plan. Harvey fitting of the Mie scattering for a cleanliness level of 300 is shown in Table 12. Simulations of the infield configuration have been done for 400 nm and 900 nm wavelength producing 3.5 10^{-4} and 3.8 10^{-4} as per Contamination Scatter respectively.

Figure 19 shows the image of straylight due to the contamination at 400 nm.

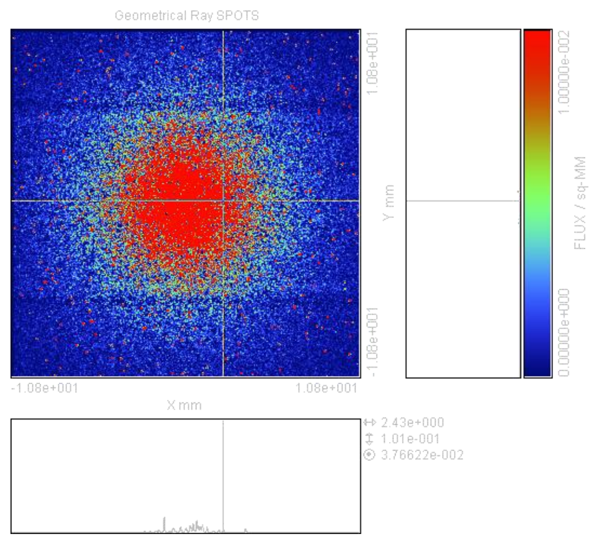

Figure 19: Straylight due to contamination 400nm.

The contamination scatter for higher level of contamination limited to the first surface is reported in Table 16.

Table 16: Contamination scattering for different value of CL on the first surface.

CL	Scatter / signal (@ 900 nm)
PPM 3165 (CL 500)	$4.9 \cdot 10^{-4}$
PPM 1265 (CL 415)	$3 \cdot 10^{-4}$
PPM 300 (CL 306)	$\mathbf{6 \cdot 10^{-5}}$

Total contamination scattering at 400 nm is $3.5 \cdot 10^{-4}$ for CL300 and $5.9 \cdot 10^{-4}$ for CL415 contamination on the first surface.

6. Summary of the scattering analysis

The straylight analysis shows that the scattering due to optical surface roughness, contamination and from mechanical items has the most important contribution at 400 nm wavelength and in field configuration: the maximum ratio of the scattered contribute with respect to the signal is $1.2 \cdot 10^{-3}$ (sum of infield, near infield, out of field and CL300 contamination). This value can be considered negligible with respect the required radiometric performance.

7. CONCLUSIONS

The high resolution channel, HRIC, of SIMBIO-SYS instrument will provide images covering up to 20% of the Mercury surface with 4 optical filters operating in the visible and near infrared spectral range.

The demanding environment of high thermal gradients around Mercury together with the scientific objectives of high spatial resolution imaging constrained to an advanced optical design. This design characterized by reduced mass and volume together with the optimized material selection and optical performances is capable to fulfill all the scientific requirements. The performed analyses on the optical quality, manufacturing tolerance sensitivity and straylight (see Table 17) allow us to predict the real operative performance of HRIC and so better planning the scientific operations at Mercury.

Table 17: This table reports the degradation budget due to the optical mounting and manufacturing tolerance, thermal and straylight effect on the instrument.

Quality Index	Mounting and Manufacturing Tol	Thermal	Straylight
RMS	< 0.13% (FoV edge)	-	-
MTF	5% (average)	< 2.1 %	negligible

Above results of these analyses confirm the high imaging capabilities of HRIC that will allow to improve present knowledge of the Mercury surface.

Funding Information.
Research Institutes acknowledge ASI support under contract I/022/10/0. The activities at Leonardo S.p.A. have been performed under ASI contract I/054/10/1.

Acknowledgments.
SIMBIO-SYS is realized by an International Consortium led by Italy and involving France for the hardware production. Leonardo is prime industrial partner.
- Dedicated to his wife Katia and their sons Emanuele, Alessandro and Andrea. Michele Zusi.
- Dedicated to his wife Patrizia and his son Matteo. Riccardo Paolinetti.

References

1. E. Flamini, F. Capaccioni, L. Colangeli, G. Cremonese, A. Doressoundiram, J. L. Josset, Y. Langevin, S. Debei, M. T. Capria, M. C. de Sanctis, L. Marinangeli, M. Massironi, E. Mazzotta Epifani, G. Naletto, P. Palumbo, P. Eng, J. F. Roig, A. Caporali, V. da Deppo, S. Erard, C. Federico, O. Forni, M. Sgavetti, G. Filacchione, L. Giacomini, G. Marra, E. Martellato, M. Zusi, M. Cosi, C. Bettanini, L. Calamai, M. Zaccariotto, L. Tommasi, M. Dami, I. Ficai Veltroni, F. Poulet, Y. Hello, Y. and the Simbio-Sys Team, "SIMBIO-SYS: The spectrometer and imagers integrated observatory system for the BepiColombo planetary orbiter", Planetary Space Sci 58(1-2), 125-143 (2010).
2. J. Benkhoff, J. van Casteren, H. Hayakawa, M. Fujimoto, H. Laakso, M. Novara, P. Ferri, H. Middleton, R. Ziethe, "BepiColombo — Comprehensive exploration of Mercury: Mission overview and science goals", Planetary Space Sci 58(1-2), 2-20 (2010).
3. G. Marra, L. Colangeli, E. Mazzotta Epifani, P. Palumbo, M. Zusi, S. Debei, E. Flamini, M. Cosi and the SIMBIO-SYS International Team, "The Optical Design of the High Resolution Imaging Channel for the SIMBIO-SYS experiment on the BepiColombo Mission to Mercury", Mem. Soc Astron Ital 12, 77-82 (2008).
4. M. Zusi, P. Palumbo, L. Colangeli, G. Marra, E. Mazzotta Epifani, V. Della Corte, C. Molfese, E. Flamini, "Observing Mercury with the High Resolution Imaging Channel of SIMBIO-SYS", Proceedings of European Planetary Science Congress (EPSC, 2010), 695 (2010).
5. V. Da Deppo, G. Naletto, G. Cremonese, L. Clamai, "Optical design of the single-detector planetary stereo camera for the BepiColombo European Space Agency mission to Mercury", Appl. Optics 49(15), 2910-2919 (2010)

6. F. Capaccioni, M. C. de Sanctis, G. Filacchione, G. Piccioni, E. Ammannito L. Tommasi, I. Ficai Veltroni, M. Cosi, S. Debei, L. Calamai, E. Flamini, "VIS-NIR Imaging Spectroscopy of Mercury's Surface: SIMBIO-SYS/VIHI Experiment Onboard the BepiColombo Mission", Proceedings of IEEE Transactions on geoscience and remote sensing (IEEE, 2010), 3932-3940 (2010).
7. L. Tommasi, M. Baroni, D. Borrelli, M. Dami, E. Di Carmine, R. Paolinetti, F. Boldrini, G. Cremonese, F. Capaccioni, P. Palumbo, Y. Langevin, A. Doressoundiram, S. Debei, F. Altieri, V. Da Deppo, V. Della Corte, G. Filacchione, C. Re, E. Simioni, M. Zusi, L. Colangeli, E. Flamini, F. Longo, R. Formaro, I. Ficai Veltroni, "SIMBIO-SYS for BepiColombo: key enabling technologies", Proceeding of the 68th International Astronautical Congress (IAC, 2017), 15 (2017).
8. L. Colangeli, G. Marra, E. M. Epifani, P. Palumbo, E. Flamini, S. Debei and the SIMBIO-SYS International Team, "The High Resolution Imaging Channel of the SIMBIO-SYS instrument for the BepiColombo mission to Mercury", Mem. Soc Astron Ital 9, 170-172 (2006).
9. G. Marra, L. Colangeli, E. Mazzotta Epifani, P. Palumbo, S. Debei and the SIMBIO-SYS International Team, "Optical Design of an High Resolution Imaging Channel for the BepiColombo space mission", Proc. SPIE 5962, 59621O (2005).
10. G. Marra, L. Colangeli, E. Mazzotta Epifani, P. Palumbo, S. Debei, E. Flamini, G. Naletto and the SIMBIO-SYS International Team, "The Optical Design and Preliminary Optomechanical Tolerances of the High Resolution Imaging Channel for the BepiColombo Mission to Mercury", Proc. SPIE 6273, 627328 (2006).
11. E. Friso, "Thermal effects reduction techniques for the SIMBIO-SYS scientific suite of BepiColombo mission", PhD thesis, University of Padova (2010).
12. O. N. Stavroudis, L. D. Foo, "System of reflective telescope baffles", Opt. Eng. 33(3), 675-680 (1994).
13. F. Cucciarrè, "Numerical and experimental methods for design and test of units and devices on BepiColombo mission", PhD thesis, University of Padova (2013).
14. E. Rugi-Grond, T. Weigel, A. Herren, M. Dominguez Calvo, U. Krähenbühl, D. Mouricaud, H. Vayssade, "Reflective baffle for BepiColombo mission", Proc. SPIE 10567, 1056714 (2006).
15. OpticStudio is a registered trademark of Zemax LLC, www.zemax.com.
16. D. Helder, J. Choi and C. Anderson, "On orbit Modulation Transfer Function (MTF) measurements for IKONOS and QuickBird", Civil Commercial Imagery Evaluation Workshop, https://calval.cr.usgs.gov/JACIE_files/JACIE06/Files/28Helder.pdf (2006).
17. ASAP is a registered trademark of Breault Research, www.breault.com/software/asap-nextgen.